Available online at www.sciencedirect.com
SCIENCE DIRECT®
Journal of Molecular Catalysis A: Chemical 240 (2005) 197–206
JOURNAL OF MOLECULAR CATALYSIS A: CHEMICAL
www.elsevier.com/locate/molcata

Characterization of Pt-Ru/C catalysts by X-ray absorption spectroscopy and temperature-programmed surface reaction

Din-Goa Liu, Jyh-Fu Lee *, Mau-Tsu Tang

National Synchrotron Radiation Research Center, 101 Hsin-Ann Road, Hsinchu Science Park, Hsinchu 30076, Taiwan, ROC

Received 27 January 2005; received in revised form 5 July 2005; accepted 5 July 2005
Available online 8 August 2005

Abstract

X-ray absorption spectroscopy (XAS) was employed to characterize carbon black supported Pt-Ru catalysts, which are commercially available to be utilized as the anode of polymeric-electrolyte-membrane fuel cells. Both Pt and Ru were found partially oxidized in the as-received form. Upon exposure to hydrogen at room temperature, the catalysts were completely reduced to the metallic state. The bimetallic nanoparticles on the Pt-Ru/C catalysts possess an inner core enriched in Pt, which is surrounded by a Ru-rich outer shell. Such a core–shell structure retained even at an elevated reduction temperature of 623 K. Temperature-programmed surface reaction (TPSR) was carried out to explore the reactivity of adsorbed CO toward hydrogen on various catalysts. Both the peak temperature of the TPSR profile and the amount of methane generated during the course of TPSR were sensitive to the surface composition of Pt–Ru nanoparticles. In combination of XAS and TPSR results, a slight difference in the nanostructure between two Pt-Ru/C catalysts was manifested.

Keywords: X-ray absorption spectroscopy; Temperature-programmed surface reaction; Pt-Ru/C catalyst; Fuel cell; CO chemisorption

1. Introduction

Fuel cell is a device, which can convert chemical energy directly into electric energy with high efficiency. In compliance with more and more strict environmental regulations, fuel cells have attracted extensive attention due to low emission of pollutants. Among various types of fuel cells, the polymeric-electrolyte-membrane fuel cell (PEMFC) is a promising candidate for portable and mobile power sources [1]. For PEMFC, however, either reformate or direct methanol feed (such as in DMFC [2]) usually causes a serious problem of CO poisoning on the anode consisting of Pt-based catalysts. Removal of strongly absorbed CO from the Pt surface is relatively slow so that many efforts were devoted to the development of binary or ternary alloy catalysts to facilitate this rate-determining step. Pt-Ru bimetallic catalysts have been found to exhibit satisfactory performance and are widely adopted for this purpose [3–5]. It is generally accepted that high activity of Pt-Ru bimetallic catalysts mainly comes from the bifunctional character of the alloy surface: adsorption of CO on Pt atoms and oxidative removal of CO by oxygen-like species adsorbed on adjacent Ru atoms [6,7].

The structure of bimetallic catalysts can be significantly influenced by the degree of alloying between two constituent elements. Particularly, the surface composition always plays a crucial role in determining the catalytic properties. In the present work, X-ray absorption spectroscopy (XAS) was employed to investigate the structure of two commercial Pt-Ru/C catalysts. XAS has been proved a powerful technique for characterization of bimetallic catalysts [8–11]. X-ray absorption near edge structure (XANES) can reveal the oxidation state and d-band occupancy of specific atom, while the local atomic structure can be obtained from the analysis of extended X-ray absorption fine structure (EXAFS) [12]. All the spectral information helps to correlate the electrochemical performance with the electronic and atomic structures

* Corresponding author. Tel.: +886 3 5780281x7117; fax: +886 3 5783813.
E-mail address: jflee@nsrrc.org.tw (J.-F. Lee).

1381-1169/$ – see front matter © 2005 Elsevier B.V. All rights reserved.
doi:10.1016/j.molcata.2005.07.011

when the Pt-Ru/C catalysts are utilized as the anode materials of PEMFCs. In addition to XAS, temperature-programmed surface reaction (TPSR) was carried out to probe the surface composition of Pt–Ru nanoparticles. A detailed review on the related theory and techniques of TPSR was given by Falconer and Schwarz [13]. Basically, the peak temperature of a TPSR profile can be regarded as a criterion to evaluate the specific rate or turnover frequency on the basis of single active site. Fujimoto et al. employed TPSR to study the alumina and silica supported platinum group metals [14]. It was found that the lower TPSR peak usually implied the higher specific rate. This correlation applies not only to various metals on the same support but also to the same metal on different supports [15,16]. Here, we successfully utilize the TPSR results to reflect the chemical composition of the outermost surface layer of the carbon supported Pt–Ru bimetallic nanoparticles.

2. Experimental

2.1. Catalysts

The carbon black (Cabot Vulcan XC-72R) supported Pt-Ru bimetallic catalysts were obtained either from Johnson Matthey Co. (called J-M sample hereafter) or from E-TEK Inc. (the E-T sample). Both catalysts have the same nominal loading of 20 wt% Pt and 10 wt% Ru (in an atomic ratio of 1:1). For the purpose of comparison, two monometallic catalysts, 20 wt% Pt/C and 10 wt% Ru/C, were obtained from E-TEK.

2.2. X-ray absorption spectroscopy

X-ray absorption spectra at Pt L_3-edge and Ru K-edge were, respectively, recorded at beamlines 17C1 and 01C1 of National Synchrotron Radiation Research Center, Hsinchu, Taiwan. The electron storage ring is operated at an energy of 1.5 GeV and a beam current of 120–200 mA. BL17C1 is based on a multi-pole wiggler source with a critical energy (E_c) of 2.7 keV, and BL01C1 utilizes the radiation from a superconducting wavelength shifter ($E_c = 7.5$ keV). Both beamlines employ a double Si(1 1 1)-crystal monochromator for energy selection with a resolution $\Delta E/E$ better than 2×10^{-4}. High-order harmonics are rejected by Rh or Pt-coated mirrors. These mirrors also serve to collimate (upstream) and refocus (downstream) the X-ray beam. All spectra were recorded at room temperature in a transmission mode in which the intensities of incident and transmitted X-ray beams were measured by gas-filled ionization chambers. Energy was scanned from 200 eV below the edge to 1000 eV above the edge. The catalyst powder was pressed into a slot of the stainless-steel holder and then placed in an in situ cell for treatment at desired condition [17]. To achieve the optimum thickness, i.e., spectral edge jump ($\Delta\mu x$) approaching unity, the pressed powder sample containing either 8.5 mg Pt/cm^2 or 17 mg Ru/cm^2 (respectively, for Pt L_3-edge and Ru K-edge measurements) across the beam was used. A standard compound, Pt foil or Ru powder, was measured simultaneously by using the third ionization chamber so that energy calibration could be performed scan by scan.

Raw X-ray absorption data were analyzed following standard procedures, including pre-edge and post-edge background subtractions, normalization with respect to the edge jump, Fourier transformation and non-linear least-squares curve fitting. Detailed description of the procedure was given elsewhere [18]. All the computer programs were implemented in the software package UWXAFS 3.0 [19]. The backscattering amplitude and phase shift for specific atom pairs were ab initio calculated by using the FEFF6 code [20,21].

2.3. CO chemisorption and temperature-programmed surface reaction (TPSR)

Catalyst powder of 0.1 g was packed between two plugs of quartz wool on the outlet side of a Pyrex U-shaped tube and purged with a hydrogen stream of 30 mL/min. Temperature was raised to 623 K at a rate of 10 K/min. After treatment at 623 K for 2 h, the catalyst was cooled in hydrogen to room temperature. Subsequently, CO pluses of 0.1 mL were repeatedly injected into the carrier gas (H_2) stream flowing through the catalyst bed until the breakthrough was observed. Two consecutive pulses were separated by an interval of 2 min. Typically, 5–15 pulses were required before the thermal conductivity detector (TCD) signal reached a constant value. With the saturated uptake of CO, the catalyst was heated in hydrogen again at 10 K/min to perform the TPSR. The effluent gas from the catalyst bed during the course of TPSR was continuously monitored by both TCD and flame ionization detector (FID).

3. Results and discussion

3.1. X-ray absorption spectroscopy

The XANES spectra for various monometallic and bimetallic catalysts in the as-received state are shown in Fig. 1. Reference spectra of some standard compounds are over-plotted for comparison. In general, the intensity of "white line" at Pt L_3-edge can reveal the degree of occupancy of 5d-electron states of the Pt atoms, which is in turn affected by the oxidation state [22]. The more intense white line implies the higher degree of oxidation. Accordingly, the Pt atoms on all catalysts were found partially oxidized because the white line intensities are between those of Pt foil and PtO_2 (the white line peak of PtO_2, not shown here, is slightly higher than 2.0 in the normalized absorption scale). It is interesting to note that the degree of oxidation of the Pt atoms on the Pt/C catalyst is higher than that on bimetallic catalysts, and that the J-M sample, as compared to the E-T sample, has more oxidized Pt. One possibility is that the

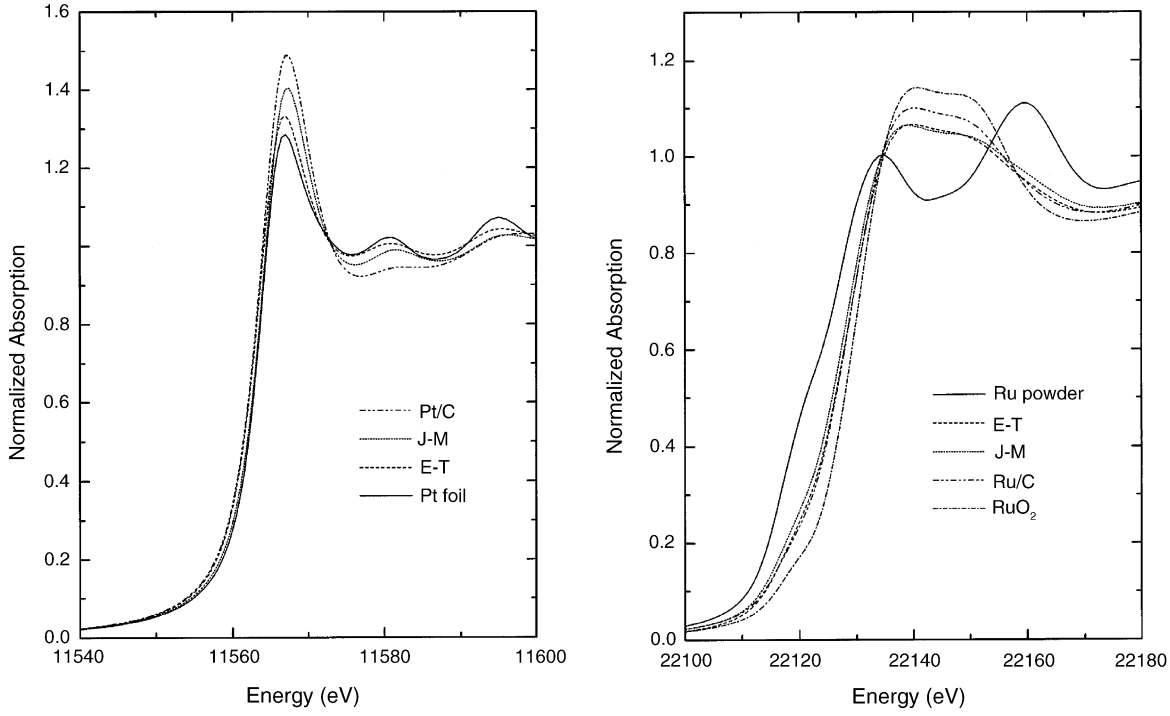

Fig. 1. XANES spectra at Pt L_3-edge (left panel) and Ru K-edge (right panel) for various samples in the as-received form.

Pt/C catalyst, in the absence of Ru atoms on the surface, possesses a larger number of surface Pt atoms being oxidized by air. For bimetallic catalysts, a significant portion of surface might be occupied by Ru atoms. The oxidized surface layer may prevent the interior atoms from further oxidation so that the average degree of oxidation of Pt became lower. Based on the same inference, the percentage of Pt atoms on the surface of the J-M sample seems higher than that on the E-T sample if both samples have similar particle sizes.

From the chemical shift in threshold energy at Ru K-edge (see the right panel of Fig. 1), it is revealed that the average oxidation number of Ru atoms was close to 3+ on either Ru/C or Pt-Ru/C catalysts. This evidence might indicate that most Ru atoms are located on the surface layer of bimetallic nanoparticles, leading to nearly the same degree of oxidation of Ru as of the monometallic catalyst. Nevertheless, a careful comparison between the threshold energies for two bimetallic catalysts showed that the average oxidation number of Ru atoms on the E-T sample is slightly higher than that on the J-M sample. This evidence implies a higher percentage of Ru atoms on the surface of the E-T sample than that of the J-M sample.

Fig. 2 presents the XANES spectra of the catalysts after exposure to hydrogen at room temperature. Judging from the white line intensity at Pt L_3-edge and the threshold energy at Ru K-edge, it is readily known that two bimetallic catalysts (J-M and E-T) are completely reduced. The spectra for the J-M and E-T samples match each other quite well; therefore, only the J-M spectrum is shown. The monometallic catalyst Pt/C exhibits a white line at Pt L_3-edge even less intense than the Pt foil, suggesting the presence of metal–support interactions. For the Ru/C catalyst, the metal–support interactions seem much weaker in view of almost identical spectral features between Ru/C and reference Ru powder.

The k^3-weighted EXAFS χ data are depicted in Fig. 3 for bimetallic catalysts either in the as-received state or after exposure to hydrogen at room temperature. Signal-to-noise ratio of the data is high enough to allow a relatively large k-range of data (from 3 to 14 Å^{-1}) to be used in the subsequent Fourier transformation and fitting. Structural parameters derived from the EXAFS data analysis at Pt L_3-edge and Ru K-edge are listed in Tables 1 and 2, respectively. The EXAFS data for the two edges were fitted simultaneously, with the interatomic distances of unlike pairs ($R_{\text{Pt-Ru}}$ and $R_{\text{Ru-Pt}}$) being set equal. For the Pt–Ru (1:1) bimetallic nanoparticles in the reduced state, the coordination numbers of unlike atom pairs ($N_{\text{Pt-Ru}}$ and $N_{\text{Ru-Pt}}$) were further constrained to match each other. This relationship is always physically valid and independent of the structural details. According to repeated fitting procedures with different initial guess values, the uncertainty of final results was found to be less than 15% in coordination number and roughly 1% in interatomic distance.

In the as-received state, the number of Pt–O bonding ($N_{\text{Pt–O}}$) on the Pt/C catalyst is significantly larger than the corresponding value for bimetallic catalysts (see Table 1). This evidence indicates a greater extent of oxidation of Pt atoms on the Pt/C catalyst, in agreement with the observation from XANES spectra. In contrast, the difference in $N_{\text{Ru–O}}$ values among various catalysts is much smaller (Table 2). One might

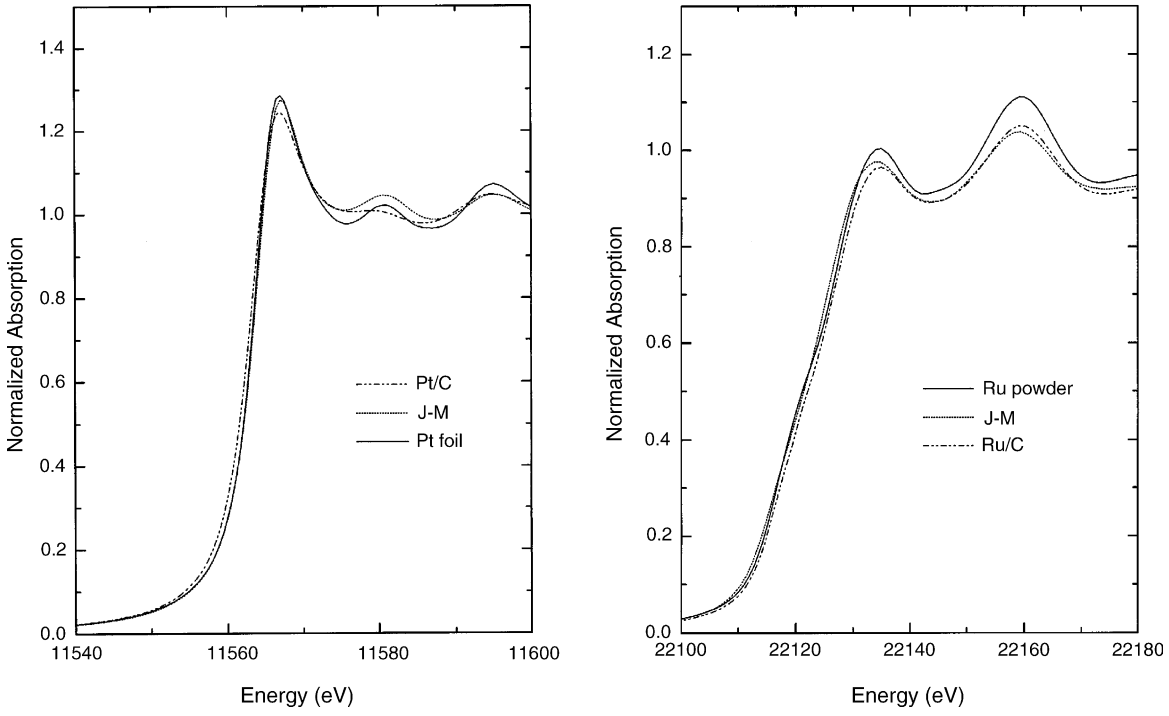

Fig. 2. XANES spectra at Pt L_3-edge (left panel) and Ru K-edge (right panel) for various samples after exposure to H_2 at room temperature.

infer that on bimetallic catalysts a large portion of Ru atoms reside on the surface of the nanoparticles. Such a speculation is evidenced by the relatively larger $N_{Ru–O}$ value than the $N_{Pt–O}$ value observed for the same bimetallic catalyst.

Upon exposure to hydrogen at room temperature, the M–O (M = Pt or Ru) bonding is no longer observable on the Ru/C and bimetallic catalysts, indicating a complete reduction. The only exception is the Pt/C catalyst on which the contribu-

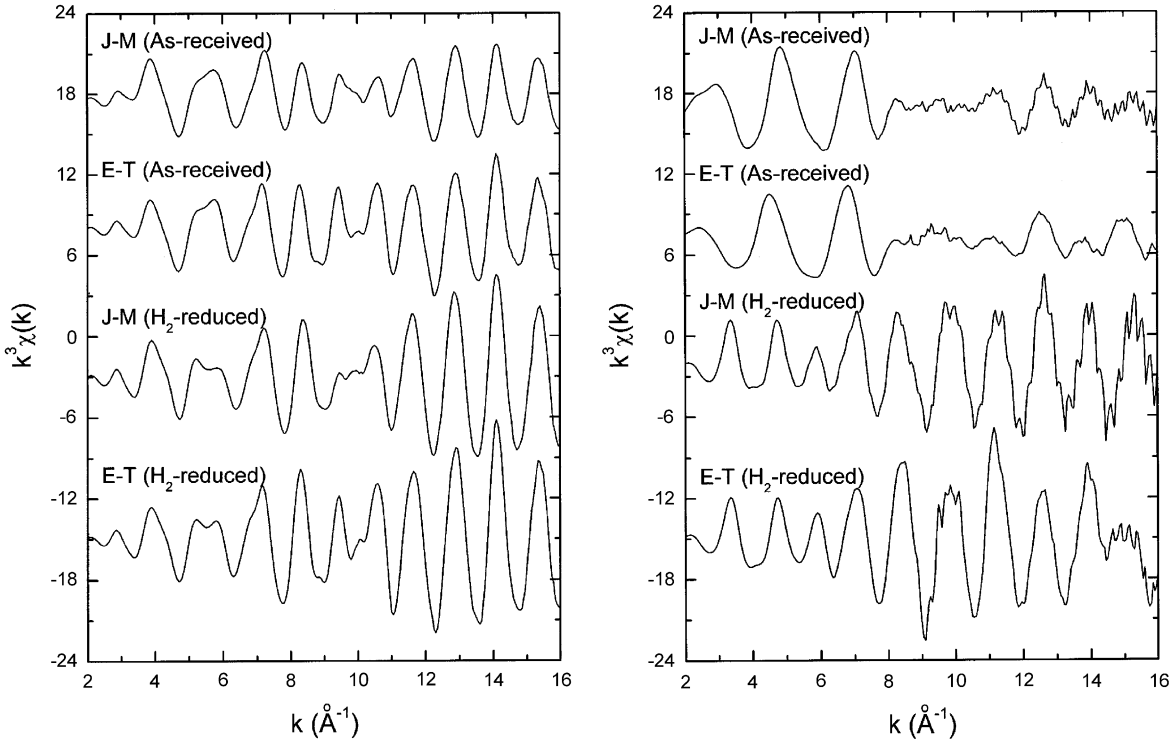

Fig. 3. k^3-weighted EXAFS data at Pt L_3-edge (left panel) and Ru K-edge (right panel) for the J-M and E-T samples each before and after exposure to H_2 at room temperature. Each set of oscillations is displaced vertically for clarity.

Table 1
Curve-fitting results of the EXAFS data at Pt L_3-edge

Sample	Bond	N	R (Å)	σ^2 (Å^2)	r-Factor (%)
J-M (as-received)	Pt–O	1.1	2.01	0.0051	0.80
	Pt–Ru	2.1	2.73	0.0070	
	Pt–Pt	4.8	2.74	0.0061	
J-M (H_2, 300 K)	Pt–Ru	2.8	2.70	0.0054	0.11
	Pt–Pt	6.5	2.74	0.0057	
J-M (H_2, 473 K)	Pt–Ru	3.0	2.71	0.0052	0.15
	Pt–Pt	6.4	2.74	0.0057	
J-M (H_2, 623 K)	Pt–Ru	2.9	2.71	0.0048	0.13
	Pt–Pt	6.5	2.73	0.0057	
E-T (as-received)	Pt–O	0.7	1.97	0.0073	0.39
	Pt–Ru	1.4	2.72	0.0064	
	Pt–Pt	6.2	2.75	0.0063	
E-T (H_2, 300 K)	Pt–Ru	2.0	2.70	0.0057	0.07
	Pt–Pt	7.5	2.74	0.0057	
E-T (H_2, 473 K)	Pt–Ru	2.1	2.68	0.0048	0.24
	Pt–Pt	7.4	2.74	0.0059	
E-T (H_2, 623 K)	Pt–Ru	2.3	2.70	0.0055	0.14
	Pt–Pt	7.1	2.74	0.0057	
Pt/C (as-received)	Pt–O	2.0	2.01	0.0047	0.48
	Pt–Pt	4.8	2.76	0.0070	
Pt/C (H_2, 300K)	Pt–O	1.0	2.21	0.0034	0.07
	Pt–Pt	8.3	2.75	0.0062	
Pt/C (H_2, 473K)	Pt–O	0.9	2.22	0.0032	0.06
	Pt–Pt	8.4	2.75	0.0060	
Pt/C (H_2, 623K)	Pt–O	0.6	2.19	0.0030	0.09
	Pt–Pt	8.7	2.75	0.0061	

Notation: N, coordination; R, interatomic distance; σ^2, Debye–Waller factor.

tion from Pt–O bonding is not negligible in the EXAFS data fitting. This type of bonding might originate from the interactions between Pt atoms and oxygen-containing groups on the surface of carbon black.

Sinfelt et al. conducted a series of EXAFS investigations on bimetallic catalyst systems with various bulk miscibilities between two constituent elements [8–10]. In their studies, segregation of like atoms commonly occurred in which one element showed a preference at the surface while the other at the core of the nanoparticles. Generally, the first-shell coordination number (counting both like and unlike atom pairs) would be larger for the element enriched in the core. Besides, the element which is enriched in the core, always exhibits a stronger preference for the selection of homometallic bonding (a higher degree of segregation) than the other element. Such a core–shell structure becomes more distinct as the bulk miscibility gets lower. Furthermore, the metal with lower surface energy tends to segregate on the surface in the thermodynamically stable phase. In the case of partial miscibility, as in the Pt–Ru system [23], the core–shell boundary would be relaxed to some extent so that the formation of heterometallic bonding becomes increasingly preferable.

Fig. 4 displays the radial distribution functions obtained by taking Fourier transform (without phase correction) of $k^3\chi$ for various catalysts after H_2 reduction at room temperature. The numerical fittings are carried out with regard to the data in r-space ranging from 1.5 to 3.0 Å. For the H_2-reduced J-M sample, Pt atoms show a clear preference for the selection of homometallic bonding ($N_{Pt\text{-}Pt} = 6.5$) over heterometallic bonding ($N_{Pt\text{-}Ru} = 2.8$). At the same time, the number of homometallic bonding between Ru atoms ($N_{Ru\text{-}Ru} = 4.1$) is also larger than the number of heterometallic bonding ($N_{Ru\text{-}Pt} = 2.8$). In view of the fact that Pt atoms exhibit a stronger preference of homometallic bonding and there are more nearest neighboring atoms around Pt center, the Pt–Ru nanoparticles were thought to possess an inner core enriched in Pt and an outer shell enriched in Ru. The number of nearest neighbors around Pt atom and Ru atom are 9.3 and 6.9, respectively, giving an averaged first-shell coordination number of 8.1. This value corresponds to an average particle size of about 20 Å on the assumption of close-packed structure [24,25]. For the E-T sample after exposure to H_2 at room temperature, EXAFS parameters show an even higher preference for the homometallic bonging, suggesting the segregation of like atoms to a greater extent. In other words, the E-T sample has a surface with higher percentage of Ru atoms than does the J-M sample. The average size of E-T bimetallic particles is comparable to that of the J-M sample, since

Table 2
Curve-fitting results of the EXAFS data at Ru K-edge

Sample	Bond	N	R (Å)	σ^2 (Å^2)	r-Factor (%)
J-M (as-received)	Ru–O	4.9	1.98	0.0106	1.10
	Ru–Ru	1.6	2.67	0.0071	
	Ru–Pt	1.6	2.73	0.0059	
J-M (H_2, 300 K)	Ru–Ru	4.1	2.65	0.0062	0.73
	Ru–Pt	2.8	2.70	0.0058	
J-M (H_2, 473 K)	Ru–Ru	4.2	2.65	0.0053	0.60
	Ru–Pt	3.0	2.71	0.0057	
J-M (H_2, 623 K)	Ru–Ru	5.1	2.66	0.0058	0.81
	Ru–Pt	2.9	2.71	0.0052	
E-T (as-received)	Ru–O	3.8	2.00	0.0088	0.42
	Ru–Ru	1.8	2.66	0.0086	
	Ru–Pt	1.5	2.72	0.0072	
E-T (H_2, 300 K)	Ru–Ru	5.0	2.65	0.0062	0.59
	Ru–Pt	2.0	2.70	0.0057	
E-T (H_2, 473 K)	Ru–Ru	5.2	2.66	0.0058	0.77
	Ru–Pt	2.1	2.68	0.0039	
E-T (H_2, 623 K)	Ru–Ru	5.7	2.66	0.0060	0.91
	Ru–Pt	2.3	2.70	0.0053	
Ru/C (as-received)	Ru–O	4.3	1.99	0.0077	1.05
	Ru–Ru	2.0	2.68	0.0088	
Ru/C (H_2, 300K)	Ru–Ru	10.0	2.67	0.0060	0.23
Ru/C (H_2, 473K)	Ru–Ru	10.0	2.67	0.0059	0.31
Ru/C (H_2, 623K)	Ru–Ru	9.9	2.67	0.0059	0.63

Notation as in Table 1.

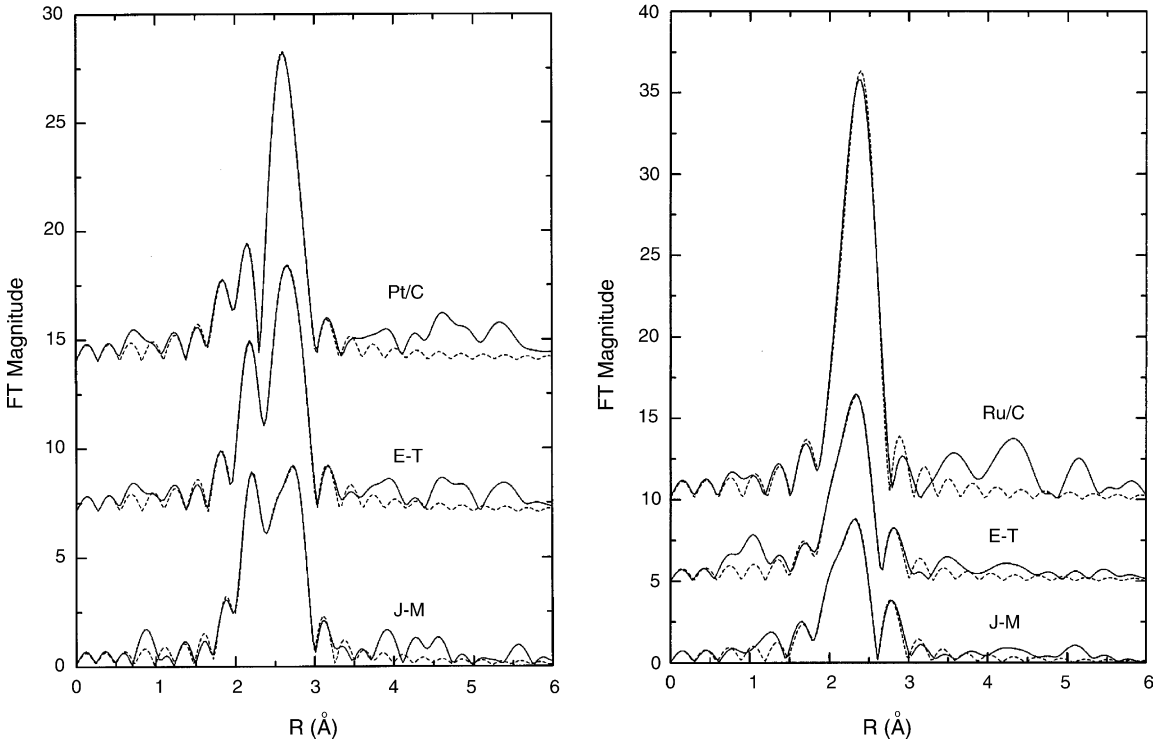

Fig. 4. Fourier transform of k^3-weighted EXAFS data at Pt L_3-edge (left panel) and Ru K-edge (right panel) for monometallic and bimetallic catalysts after exposure to H_2 at room temperature. Solid line denotes the experimental data and dashed line shows the computer fit.

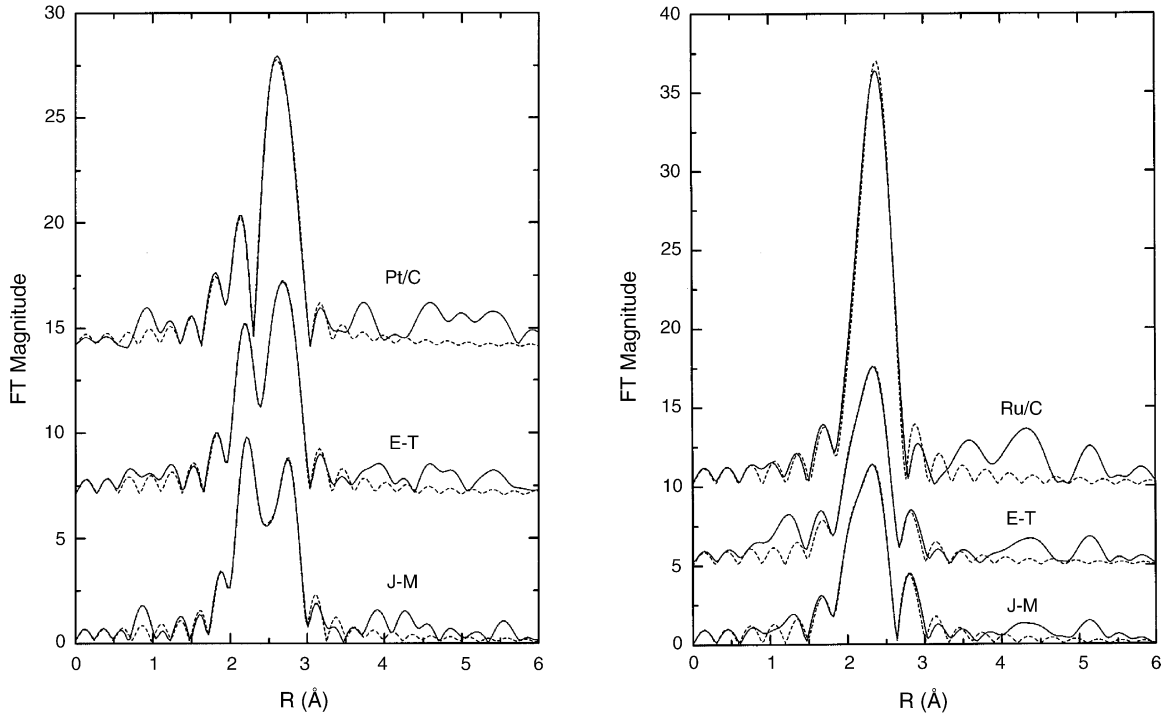

Fig. 5. Fourier transform of k^3-weighted EXAFS data at Pt L_3-edge (left panel) and Ru K-edge (right panel) for monometallic and bimetallic catalysts after reduction by H_2 at 623 K. Solid line denotes the experimental data and dashed line shows the computer fit.

both catalysts have roughly the same first-shell coordination number.

Nashner et al. utilized molecular cluster precursor $PtRu_5C(CO)_{16}$ to prepare the carbon-supported Pt–Ru nanoparticles via reductive condensation [26,27]. Pt atoms were found preferentially at the core of the incipient Pt–Ru nanoparticles. After further high-temperature treatment in H_2 to 673 K, the nanoparticles adopted an inverted structure in which Pt atoms appeared preferentially at the surface. In fact, such a core–shell inversion is expectable because the surface energy of Pt is slightly lower than that of Ru [28]. For equilibrated Pt–Ru nanoparticles, the surface should be enriched in Pt atoms [29]. It is interesting to find that both J-M and E-T samples possess Pt–Ru nanoparticles with a Pt-rich core and a Ru-rich shell in this work. Such a nanostructure is obviously non-equilibrated. Attempts were made to raise the temperature of H_2 treatment progressively to 473 and 623 K, but no core–shell inversion eventually occurred (see the corresponding structural parameters in Tables 1 and 2). The average particle size of bimetallic catalysts becomes slightly larger after high-temperature treatment, as reflected by the first-shell coordination number particularly from the viewpoint of Ru center. Fig. 5 shows the radial distribution functions for the catalysts after being subjected to H_2-treatment at 623 K for 2 h. Intraparticle atomic rearrangement can be clearly identified by comparing Fig. 5 with Fig. 4. Relative to the room-temperature H_2-treated catalysts, the structural parameters for high-temperature treated bimetallic catalysts show a slightly higher preference for heterometallic bonding, indicating a higher degree of intermixing between Pt and Ru atoms. This state may be regarded as an intermediate state before final core–shell inversion. However, for the Pt–Ru nanoparticles of an average size nearly 20 Å in this work, complete core–shell inversion requires either higher temperature or longer period.

3.2. CO chemisorption and temperature-programmed surface reaction

The CO uptake was measured by means of the flow method in which hydrogen was selected as the carrier gas. In contrast to the static (volumetric) method, the flow method usually gives the amount of strongly adsorbed CO. One advantage of using hydrogen instead of other inert gases as the carrier gas is to prevent the catalyst surface from being oxidized by any oxygen-containing impurities in the stream. In view of the fact that subsequent TPSR would be carried out in hydrogen, the choice of hydrogen carrier gas for CO chemisorption also eliminated the need of switching between different gas streams. It was reported that the CO uptake measured in hydrogen is sometimes larger than that measured in helium [30]. In those cases, hydrogen acted as a promoter rather than a competitor for CO adsorption on metal surfaces.

The amounts of CO chemisorption on various samples are listed in Table 3. It is interesting to note that the Ru/C catalyst exhibited a capacity for CO adsorption four times larger than the Pt/C catalyst although the former has a slightly larger particle size than the latter (as reflected by the EXAFS data). Accordingly, large discrepancy in CO uptake between these two monometallic catalysts is attributable to the substantial

Table 3
Summary of CO chemisorption and TPSR results

Sample	CO uptake (μmol/g)	TPSR peak temperature (K)	CH_4 generated during TPSR (μmol/g)
Pt/C	92	–	–
Ru/C	390	481	269
Physical mixture[a]	211	483	150
E-T	276	546	149
J-M	219	>623	25

[a] Pt/C and Ru/C catalysts in a ratio of 1:1 by weight.

difference in the stoichiometry of adsorbed CO on surface atom.

As expected, the physical mixture of 10% Ru/C and 20% Pt/C catalysts (in a ratio of 1:1 by weight) has a saturated CO uptake being roughly half the sum of CO uptakes on individual catalysts. With regard to the two bimetallic Pt-Ru/C catalysts, the E-T sample exhibits a significantly larger CO uptake than the J-M sample does. Because the Pt–Ru particle size of the E-T sample is comparable to that of the J-M sample, as discussed above, it is speculated that the E-T sample possesses a surface of a higher Ru percentage, compared to the J-M sample.

Following CO chemisorption, the catalyst was heated in hydrogen at a rate of 10 K/min to perform the TPSR. Fig. 6 presents the TPSR profiles recorded from the FID and TCD signals. FID is well known to be very sensitive to organic molecules, whereas inorganic compounds produce negligible FID signals. Since hydrogen was always in large excess with respect to surface-adsorbed CO during the TPSR, the FID signal should mostly result from the generation of methane (the formation of other long-chain hydrocarbons would be negligible). In other words, the TPSR profile recorded from the FID signal is the curve of methane generation rate versus process temperature. At the same time, the TCD signal served to be complementary to the FID signal. Thermal desorption of CO molecules can be easily detected by TCD.

The Ru/C catalyst exhibits a very sharp peak at 481 K on the TPSR profile. The asymmetric shape (in which the lower-temperature side is less steep) of this peak might be an indication of first-order kinetics [13]. A little bump appeared at temperatures higher than 600 K. A blank test confirmed that decomposition of surface organic groups on the carbon black is responsible for this bump. In addition, a small portion (<5%) of CO directly escaping from the surface at the initial stage of the temperature program can be seen from the TCD signal (the right panel of Fig. 6).

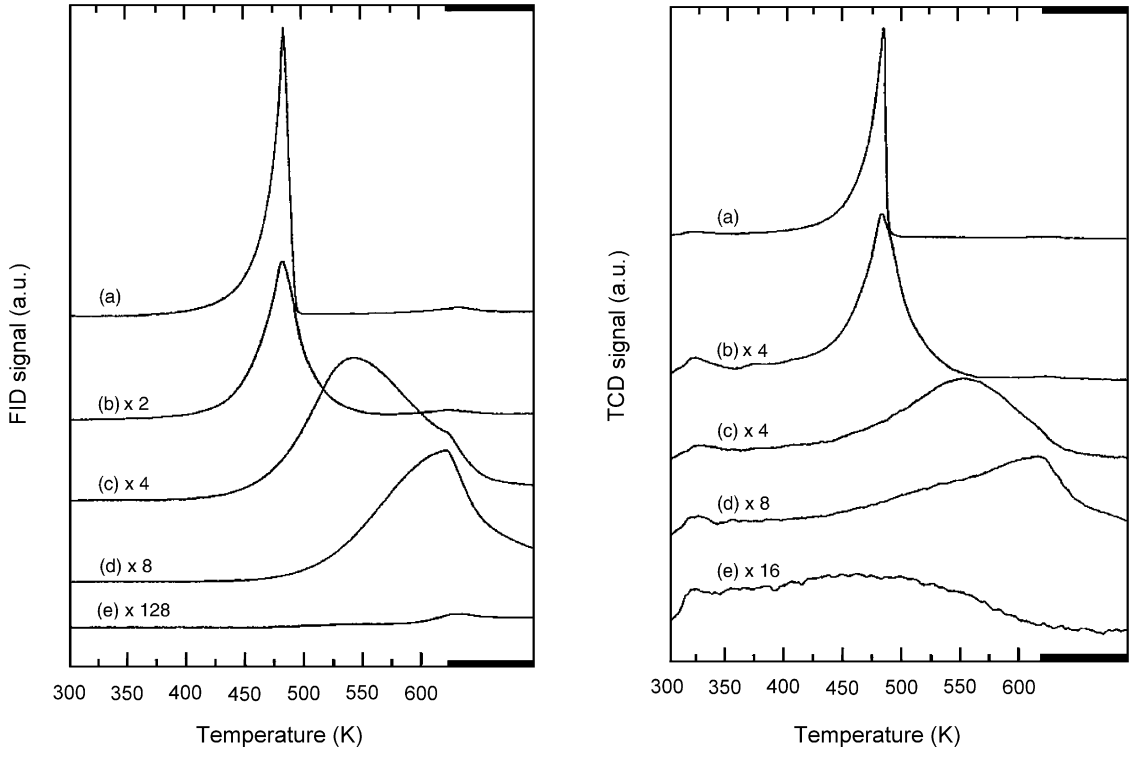

Fig. 6. TPSR profiles recorded from the FID signal (left panel) and TCD signal (right panel) for (a) Ru/C, (b) physical mixture of Pt/C and Ru/C, (c) E-T, (d) J-M and (e) Pt/C. Temperature was raised at 10 K/min to 623 K and then kept constant. The number following each label denotes the relative amplification factor for plotting the corresponding profile.

The TPSR profile of the Pt/C catalyst showed no methane formation at all. The TCD signal indicates that almost all surface-adsorbed CO undergoes thermal desorption rather than hydrogenation. Molecule balance based on TCD signals on CO adsorption and desorption is quite good (less than 10% mismatch). Moreover, CO desorption peak is relatively broad. A significant portion of CO molecules seemed strongly stuck onto the Pt surface and can only be removed at temperatures higher than 500 K. Such an observation that no methane was formed during the TPSR is completely beyond expectation, because Pt has long been known as a good catalyst for CO hydrogenation [15,16]. Furthermore, the TPSR result for the Pt/C catalyst in this study is different from the results obtained on Al_2O_3 or SiO_2 supported Pt catalysts where a TPSR peak clearly appeared [14]. This peculiar phenomenon may originate from the support effect and deserves future investigation. At this moment, nevertheless, these two extremes of TPSR results obtained on Ru/C and Pt/C catalysts form a basis for comparisons among various Pt-Ru/C catalysts.

Peak temperature of the TPSR profile for the physical mixture of Pt/C and Ru/C is almost the same as that for Ru/C catalyst alone. In fact, this result can be utilized as a criterion to judge whether phase separation occurs in bimetallic Pt-Ru/C catalysts. If some isolated Ru clusters exist, a TPSR peak around 480 K should be observable. For this physical mixture, the TPSR profile shows a peak with more symmetric shape. The tailing feature on the high-temperature side is attributable to some CO molecules originally adsorbed on Pt surface, which move to Ru surface (via desorption–readsoption process) and are hydrogenated later. Such a speculation is further supported by the fact that the ratio of methane formed in TPSR to original CO uptake is slightly higher on the physical mixture than on the Ru/C catalyst.

A broad peak appeared at 546 K on the TPSR profile of the E-T sample. In view of the absence of a TPSR peak around 480 K, all Ru atoms seemed “alloyed” with Pt atoms to form Pt–Ru bimetallic particles on this sample. The TPSR behavior, in terms of peak temperature and amount of methane formed, is in between two monometallic catalysts. Note that the process temperature was raised to 623 K and kept there isothermally for a period of time. The loss of further driving force leads to a shoulder-like feature on the descending part of the TPSR profile.

Following similar inference from the TPSR results, percentage of Pt atoms on the surface of the J-M sample should be higher as compared with the E-T sample. Specifically, the TPSR peak temperature seems to be higher than 623 K for the J-M sample so that the end point of temperature program was not high enough to see the real TPSR peak. Besides, the ratio of methane formed in TPSR to original CO uptake is relatively low on this sample. In summary, the higher difficulty for CO to be hydrogenated on the J-M sample reflects a surface with more Pt-like characteristics, consistent with the XAS results.

4. Conclusions

X-ray absorption spectroscopy and temperature-programmed surface reaction have been employed to characterize two commercial Pt-Ru/C catalysts. Once reduced by hydrogen at room temperature, the Pt–Ru bimetallic nanoparticles on both samples possess a Pt-rich core surrounded by a shell enriched in Ru. Such a structure is quite stable: no core–shell inversion occurs even after being treated at 623 K. Both peak temperature and peak area of the TPSR profile are sensitive to the surface composition of Pt–Ru nanoparticles. The percentage of Pt atoms on the surface of the J-M sample is found to be higher than that of the E-T sample, which is in good agreement with the XAS evidence. The different surface composition successfully revealed may be of great value in accounting for the different electrochemical performances exhibited by these two catalysts.

Acknowledgments

Preliminary XAS measurements at Ru K-edge were carried out at BL12B2 of SPring-8, Japan. Financial support of this research by National Science Council, Republic of China, under contract numbers NSC 91-2113-M-213-004 and NSC 92-2113-M-213-003 was gratefully acknowledged.

References

[1] B.C.H. Steele, A. Heinzel, Nature 414 (2001) 345.
[2] B.D. McNicol, D.A.J. Rand, K.R. Williams, J. Power Sources 83 (1999) 15.
[3] M. Watanabe, M. Uchida, S. Motoo, J. Electroanal. Chem. 229 (1987) 395.
[4] S.D. Lin, T.-C. Hsiao, J.-R. Chang, A.S. Lin, J. Phys. Chem. B 103 (1999) 97.
[5] T. Page, R. Johnson, J. Hormes, S. Noding, B. Rambabu, J. Electroanal. Chem. 485 (2000) 34.
[6] H.A. Gasteiger, N. Markovic, P.N. Ross Jr., E.J. Cairns, J. Phys. Chem. 97 (1993) 12020.
[7] T. Frelink, W. Visscher, J.A.R. van Veen, Surf. Sci. 335 (1995) 353.
[8] J.H. Sinfelt, G.H. Via, F.W. Lytle, Catal. Rev. Sci. Eng. 26 (1984) 81.
[9] G.H. Via, K.F. Drake Jr., G. Meitzner, F.W. Lytle, J.H. Sinfelt, Catal. Lett. 5 (1990) 25.
[10] G.H. Via, J.H. Sinfelt, in: Y. Iwasawa (Ed.), X-ray Absorption Fine Structure for Catalysts and Surfaces, World Scientific, Singapore, 1996, p. 147 (Chapter 7.1).
[11] N. Toshima, T. Yonezawa, New J. Chem. 22 (1998) 1179.
[12] D.C. Koningsberger, R. Prins (Eds.), X-ray Absorption: Principles, Applications, Techniques of EXAFS, SEXAFS, and XANES, John Wiley & Sons, New York, 1988.
[13] J.L. Falconer, J.A. Schwarz, Catal. Rev. Sci. Eng. 25 (1983) 141.
[14] K. Fujimoto, M. Kameyama, T. Kunugi, J. Catal. 61 (1980) 7.
[15] M.A. Vannice, J. Catal. 37 (1975) 449.
[16] M.A. Vannice, J. Catal. 50 (1977) 228.
[17] F.W.H. Kampers, T.M.J. Maas, J. van Grondelle, P. Brinkgreve, D.C. Koninsberger, Rev. Sci. Instrum. 60 (1989) 2635.
[18] H.-Y. Lee, T.-B. Wu, J.-F. Lee, J. Appl. Phys. 80 (1996) 2175.

[19] E.A. Stern, M. Newville, B. Ravel, Y. Yacoby, D. Haskel, Phys. B 208–209 (1995) 117.
[20] J.J. Rehr, R.C. Albers, S.I. Zabinsky, Phys. Rev. Lett. 69 (1992) 3397.
[21] J.J. Rehr, Jpn. J. Appl. Phys. 32 (1993) 8.
[22] J.H. Sinfelt, G.D. Meitzner, Acc. Chem. Res. 26 (1993) 1.
[23] J.M. Hutchinson Jr., Platinum Met. Rev. 16 (1972) 88.
[24] B.C. Gates, J.R. Katzer, G.C. Schuit, Chemistry of Catalytic Process, McGraw-Hill, New York, 1979.
[25] R.B. Greegor, F.W. Lytle, J. Catal. 63 (1980) 476.
[26] M.S. Nashner, A.I. Frenkel, D.L. Adler, J.R. Shapley, R.G. Nuzzo, J. Am. Chem. Soc. 119 (1997) 7760.
[27] M.S. Nashner, A.I. Frenkel, D. Somerville, C.W. Hills, J.R. Shapley, R.G. Nuzzo, J. Am. Chem. Soc. 120 (1998) 8093.
[28] H.A. Gasteiger, P.N. Ross Jr., E.J. Cairns, Surf. Sci. 293 (1993) 67.
[29] P.K. Babu, H.S. Kim, E. Oldfield, A. Wieckowski, J. Phys. Chem. B 107 (2003) 7595.
[30] K.B. Kester, J.L. Falconer, J. Catal. 89 (1984) 380.